Journal of Quantitative Spectroscopy & Radiative Transfer 354 (2026) 109833

Contents lists available at ScienceDirect

Journal of Quantitative Spectroscopy and Radiative Transfer

journal homepage: www.elsevier.com/locate/jqsrt

An assigned room temperature line list for $H_2{}^{16}O$☆

Nikolai F. Zobov [a], Irina I. Mizus [a], Roman I. Ovsyannikov [a], Mikhail A. Rogov [a,b], Jonathan Tennyson [c,*], Marco Pezzella [d], Sergei N. Yurchenko [c], Robert R. Gamache [e], Oleg L. Polyansky [c,a]

[a] Institute of Applied Physics, Russian Academy of Sciences, Ulyanov Street 46, Nizhny Novgorod, 603950, Russia
[b] Department of Radiophysics, N. I. Lobachevsky State University of Nizhny Novgorod, 23 Gagarin Avenue, Nizhny Novgorod 603022, Russia
[c] Department of Physics and Astronomy, University College London, Gower Street, London WC1E 6BT, UK
[d] École Polytechnique de Lausanne, Switzerland
[e] Department of Environmental, Earth, and Atmospheric Sciences, University of Massachusetts Lowell, 265 Riverside Street, Lowell 01854, USA

ARTICLE INFO

Dataset link: https://doi.org/10.1016/j.jqsrt.2025.109620

Keywords:
Water line list
Potential energy surface
Variational nuclear motion calculations
Quantum number assignments
MARVEL energy levels

ABSTRACT

Water line list UCLH2O296 for HITRAN database has been calculated using the new global composite potential energy surface, named PES40K, obtained similarly as POKAZATEL PES by improving 246 polynomial coefficients. Nuclear motion calculations were performed using DVR3D in Radau coordinates.The PES optimization procedure was based on a method proposed by Yurchenko et al. which optimizes simultaneously with respect to both empirical energy levels and ab initio energies. Transition Intensities for the UCLH2O296 line list were computed using the ab initio CKAPTEN DMS of Conway et al. Our calculation gave 477 395 transitions up to 44500 cm^{-1} involving 241 234 states with $J \leq 26$. To label the energy levels with rovibrational quantum numbers J, K_a, K_c, v_1, v_2, and v_3, a complex procedure as a combination of 5 methods ((A) Wavefunction contribution, (B) Nodes counting, (C) Modified Hose–Taylor method, (D) Labeling merging and correction, (E) Correction by $E(K_a)$ dependencies) is developed and applied to a line list. Vibrational labeling using the Wavefunction contribution method (TROVE program) is more accurate, while rotational labeling is more accurate using the modified Hose–Taylor method. At total of 92 035 levels are now labeled by K_a, K_c and v_2 quantum numbers, and 48 440 of these 92 035 levels were labeled fully by K_a, K_c, v_1, v_2 and v_3. Line shape coefficients are a result of a "diet" procedure. Comparisons with existing $H_2{}^{16}O$ line lists are given.

1. Introduction

Water molecule is arguably the most important polyatomic molecule in the entire Universe as well as being molecule number one in the HITRAN database. Its spectrum is very well studied, see [1] for a recent comprehensive overview.

Applications of water spectra are wide-ranging: for example atmospheric science, metrology and astrophysics all require as accurate a knowledge of the line positions and line intensities as possible. Comprehensive information on the rovibrational spectrum of water is therefore of high importance for the numerous scientific and technical applications. Any improvement in this direction is thus also important. The MARVEL (Measured Active Rotation-Vibration Energy Levels) procedure [2,3] has been used to determine $H_2{}^{16}O$ empirical energy levels and hence line positions in a series of more accurate and more extensive studies [1,4–8], which aim to correspond to experimental accuracy for the line centers and sometimes supersedes them because this process provides the proper averaging of the experimental data, see [6] for example. Note that MARVEL energies can also be used to accurately predict yet to be measured transition wavenumbers [9,10]. However, many important energy levels that are yet to be characterized experimentally; these can be predicted using variational nuclear motion calculations but require improvements in the first principle model to bring the predicted values close to the actual ones. Furthermore, improvement in the potential energy surface (PES) are necessary to

☆ This article is part of a Special issue entitled: 'Memorial issue in honor of Mikhail Tretyakov' published in Journal of Quantitative Spectroscopy and Radiative Transfer.

* Corresponding author.
E-mail addresses: j.tennyson@ucl.ac.uk (J. Tennyson), o.polyansky@ucl.ac.uk (O.L. Polyansky).

https://doi.org/10.1016/j.jqsrt.2026.109833
Received 17 December 2025; Received in revised form 16 January 2026; Accepted 16 January 2026
Available online 23 January 2026

provide accurate rovibrational wavefunctions for use in calculation of accurate line intensities. Gradual improvement of the quality of the water PESes has been published in [11–16]. The construction of the global PES from [14] and Global PES [16] with a subsequent fit is presented in Section 2 of this paper.

Experimental and theoretical studies of water are converted as the "final product" of such studies to line lists. The importance of extensive hot water line lists [12,17] and globally complete hot water line lists [18] for the numerous applications, such as discovery of water in the exoplanetary atmosphere [19], is confirmed by the many hundreds of citations of each of the paper cited.

Room temperature water line lists [12,20–22] calculated in a similar manner have already been extensively used in the HITRAN database [23–25]. However, there is an issue with many of these line lists associated with the quantum numbers assigned to the various transitions and energy levels.

The attribution of the quantum numbers to the energy levels calculated by the numerical variational methods is not straightforward. For $H_2{}^{16}O$, only the total rotational angular momentum (J), parity (given by whether K_c is even or odd) and nuclear spin symmetry (given by $K_a + K_c + v_3$ is even for para states and odd for ortho ones) are rigorous quantum numbers; these last two quantum numbers can be compounded together and represented by the molecular symmetries. The division of the energy levels by symmetry makes each list of the levels four times less dense.

By convention water vibrational states are labeled using harmonic oscillator quantum numbers v_1, v_2 and v_3 which represent the degree of excitation of the symmetric stretch, bending and asymmetric modes, respectively. Although these standard quantum numbers are approximate, there are several reasons why it is useful to label energy levels with them. The set of rotation-vibration quantum numbers gives an unambiguous label for each level. These labels attribute, though approximate, physical meaning to the energy level in terms of the vibrational and rotational movement; for example (a) extreme stretching modes have strong transition dipoles associated with them and are much brighter at shorter wavelengths than other modes; (b) certain combinations of high K_a and high K_c levels are quasi-degenerate; (c) systematic issues with PES fits can be identified and addressed; (d) the labels also provide an easy means of matching variationally calculated levels with the conventional calculated energy levels from Effective Hamiltonians as well as empirical levels from MARVEL; note that the MARVEL procedure requires that each level has its own set of unique (quantum number) labels. Perhaps most importantly, quantum number labels are extensively used in line broadening calculations, in many cases these methods are based on the assignment of K_a and vibrational quantum numbers, especially v_3.

So far two approaches have been used for the very extensive line lists needed to model the spectral signature of hot water. One approach is to simply present rigorous quantum numbers only [17,18,22,26]; an alternative is to try and predict these quantum numbers on the basis of properties of the basis functions used in the calculation [12,27,28]; we note that the program TROVE [29], which is employed here, also uses this approach. The first approach clearly lacks information while second is prone to giving the same assignments to multiple levels and other related issues. In particular, we note that many assignments have been made which do not satisfy the Hose-Taylor theorem [30] that states that for assignments made using the contribution of the dominant basis function, the absolute value of its coefficient in the basis set expansion must be greater then $2^{-\frac{1}{2}}$ for the assignment to be considered correct. Clearly neither approach is satisfactory. There have been a number of other attempts to identify a comprehensive set of labels for the rovibrational levels of water [28,31–36]; none of these attempts can be regarded as having solved this problem meaning that available extensive line lists contain many levels which either are not fully assigned or contain many dubious/unreliable assignments.

There are two issues that make the provision of a full set of unique and physically meaningful quantum numbers particularly challenging for $H_2{}^{16}O$. First, it has long been established [37] that the stretching states in water switch from a normal mode structure at low levels of excitation to a local mode structure for higher values of $v_1 + v_3$. Attempts to produce water line lists labeled using basis function coefficients have particularly struggled with this transition. Second, water contains a monodromy point in its potential at linear geometries [38] which leads to standard bent molecule harmonic oscillator–rigid rotor quantum numbers not applying [39]; it is therefore unsurprising that there are issues with assigning such quantum numbers to highly excited v_2 states. Nonetheless, in this paper we try to provide a set of quantum numbers which are, as far as is possible, correct, complete and unique. These quantum numbers are then used to identify pressure broadening parameters allowing us to generate a new, complete and (substantially) assigned HITRAN-style line list. To do this first we create a new, improved line list.

The paper is organized as follows. Section 2 presents details of the functional form and optimization of our improved $H_2{}^{16}O$ PES. Section 3 presents a comparison of our calculated line centers and intensities with the previously published line lists and MARVELised energy levels. In Section 4 we describe our labeling procedure and present the results obtained for the assignment of the quantum numbers to the calculated water energy levels. Section 5 presents line shape data and Section 6 contains our conclusions.

2. Global PES

The new global potential for the main water isotopologue $H_2{}^{16}O$, which we call PES40K, has a composite structure, which is analogous to the structure of the PES used in computing the POKAZATEL line list [18]. We used the potential of Bubukina et al. [14] as the lower part V_{low} of the new PES, while the upper surface V_{up} has a functional form identical to that of the POKAZATEL PES, but with an improved set of 246 polynomial coefficients. The upper and lower potentials of PES40K, which were aligned to have the same minimum energy values, are stitched together using the approach of Varandas et al. [40]:

$$V = f_{\text{up}} \cdot V_{\text{up}} + f_{\text{low}} \cdot V_{\text{low}}, \tag{1}$$

where the switching functions:

$$f_{\text{up}} = \frac{1}{2}(1 + \tanh(\gamma \cdot \Delta E)),$$

$$f_{\text{low}} = \frac{1}{2}(1 + \tanh(-\gamma \cdot \Delta E)),$$

$$\Delta E = V_{\text{up}} - E_0,$$

$$\gamma = \gamma_0 + \gamma_1 \cdot \Delta E^2,$$

and $\gamma_0 = 1/130\,\text{cm}$, $\gamma_1 = 1/130^3\,\text{cm}^2$, $E_0 = 35\,000\,\text{cm}^{-1}$ are the nonlinear adjustable parameters of the new PES expressed in units appropriate for energies in wavenumbers. The quality of the final PES depends weakly on concrete values of γ parameters. We choose the values close to the original paper [40].

Nuclear motion calculations were performed using DVR3D [41] in Radau coordinates; they used Morse-like oscillators with the values of parameters $r_e = 3.0$, $D_e = 0.2$ and $\omega_e = 0.008$ in atomic units for both radial coordinates, and associated Legendre functions for the angular coordinate as basis functions. Corresponding DVR grids contained 60, 60 and 40 points for these coordinates, respectively. The final diagonalized vibrational matrices had a dimension of 5500. For the rotational problem, the dimensions of final matrices can be obtained as $400(J + 1 - p)$, where J is the total angular momentum quantum number and p is the rotationless parity ($p = 0$ for e and 1 for f). Nuclear masses were used and set to 15.990526 Da for the oxygen and 1.007276 Da for the hydrogen nucleus. To ensure good accuracy

for high-J calculations, we used the representation of rotational non-adiabatic effects presented by Bubukina et al. [14] with the values of corresponding adjustable parameters were left unchanged.

The PES optimization procedure was based on a method proposed by Yurchenko et al. [42] which optimizes simultaneously with respect to both empirical energy levels and *ab initio* energies. This helps to avoid nonphysical behavior of the optimized PES in regions not well characterized by the empirical levels. For this purpose we used a set of 750 *ab initio* energies in the energy region 25 000 – 45 000 cm^{-1}. In the final stages of our fit the *ab initio* points were weighted 5×10^{-4} times the weight of the empirical data. Standard deviation of our final upper PES from this set of *ab initio* data is about 52 cm^{-1}. We varied the values of 246 linear potential parameters of the upper surface V_{up}, while keeping V_{low} fixed, to obtain the highest accuracy experimental energy levels set in the energy range from 25 000 to 40 000 cm^{-1}. As a result, we obtained an upper potential, which reproduces a set of 276 experimental data with J values 0, 2 and 5 in the energy region 25 000–40 000 cm^{-1} with a standard deviation of 1.48 cm^{-1}. About 7% of the experimentally-determined energy levels in this energy region were excluded from the fit.

Then the three nonlinear switching parameters γ_0, γ_1 and E_0 were adjusted manually by a trial-and-error procedure leading to the final version of the new global potential PES40K. The overall standard deviation with which PES40K reproduces almost all the available empirical levels with $J = 0, 2, 5$ in energy range to slightly over 40 000 cm^{-1} is about 0.6 cm^{-1}. However, the most useful feature of the new PES is its accuracy at low energies. Use of PES40K reproduces 842 empirical energy levels up to 15 000 cm^{-1} with a root mean square (rms) value of 0.013 cm^{-1}, and 630 empirical energies between 15 000 and 25 000 cm^{-1} with an accuracy of 0.026 cm^{-1}. About 3.5% and 6.4% of the available experimental data in these energy ranges, respectively, were excluded from our fits. These rms values for different energy ranges, together with the number of excluded levels and the accuracy of their representation, are summarized in Table 1. Most of the excluded energy levels are highly excited or have high values of bending quantum number v_2. Table 1 also contains a comparison of the new PES40K and previously published potentials in the regions where they are defined. We note that PES40K performs approximately a factor of two better than POKAZATEL for states below 25 000 cm^{-1}.

We provide a FORTRAN implementation of PES40K, as well as the full list of outliers from its fit, in the supporting material.

2.1. The UCLH2O296 line list

Transition Intensities for the UCLH2O296 line list were computed using the *ab initio* CKAPTEN DMS of Conway et al. [43]. Our calculation gave 477 395 transitions up to 44 500 cm^{-1} involving 241 234 states with $J \leq 26$. The W2024 MARVEL level set [1] contains 19 028 levels with $J \leq 42$ and energies up to 26 267.79 cm^{-1}.

We employed a MARVELisation procedure (replacing calculated energy values by empirical values if available) [44]. MARVEL quantum numbers were adopted for 19 018 levels. The MARVEL labels for the 10 other levels strongly disagree with our wavefunction analysis results and their labels are taken from our analysis; a list of these levels is provided in the supplementary materials. For our 296 K line list using HITRAN cut-offs, all lower state energies were MARVELised. For wavenumbers below 10 000.0 cm^{-1} 101 559 upper states (97.3%) were also MARVELised. Between 10 000.0 and 25 000.0 cm^{-1}, 71 446 (45.9%) of the upper states were MARVELised and above 25 000.0 cm^{-1} only 313 (0.14%) were MARVELised, showing that more work is required at shorter wavelengths.

Table 1
Numbers (N_X^Y) of experimental energy levels with $J = 0, 2, 5$ used in our fits (X = used) and excluded from them (X = excl.) and root mean square (rms) deviations (rms_X^Y) of obs.-calc. in cm^{-1} for our new global potential PES40K, the POKAZATEL PES [18], PES of Bubukina et al. [14], and PES15K [15] for different energy ranges: up to 15 000 cm^{-1} (Y = low), 15 000–25 000 cm^{-1} (Y = mid), 25 000–45 000 cm^{-1} (Y = up), and the entire range, for which a PES was constructed: up to 45 000 cm^{-1} for PES40K and POKAZATEL, up to 25 000 cm^{-1} for Bubukina, and up to 15 000 cm^{-1} for PES15K (Y = all). In parentheses, the numbers of excluded energy level as a percentage of the total number of available empirical levels are specified.

	PES40K	POKAZATEL	Bubukina	PES15K
rms_{used}^{low}	0.0133	0.0270	0.0131	0.0112
N_{used}^{low}	842	842	842	847
rms_{used}^{mid}	0.0258	0.0507	0.0185	
N_{used}^{mid}	630	630	646	
rms_{used}^{up}	1.4838	1.4172		
N_{used}^{up}	276	276		
rms_{used}^{all}	0.5899	0.5673	0.0157	0.0112
N_{used}^{all}	1748	1748	1488	847
$rms_{excl.}^{low}$	0.3179	0.2963	0.3184	0.4351
$N_{excl.}^{low}$	31 (3.6)	31 (3.6)	31 (3.6)	26 (3.0)
$rms_{excl.}^{mid}$	0.1559	0.1284	0.1993	
$N_{excl.}^{mid}$	43 (6.4)	43 (6.4)	27 (4.0)	
$rms_{excl.}^{up}$	5.0229	4.5326		
$N_{excl.}^{up}$	20 (6.8)	20 (6.8)		
$rms_{excl.}^{all}$	2.3265	2.0994	0.2696	0.4351
$N_{excl.}^{all}$	94 (5.1)	94 (5.1)	58 (3.8)	26 (3.0)

2.2. TROVE *rovibrational calculations for water*

The variational nuclear-motion program TROVE [45] was used to compute the rovibrational energies of water employing the PES40K. Calculations were performed for rotational excitations up to $J = 60$ using an exact kinetic energy (EKE) operator. The EKE formulation is based on the bisector embedding for triatomic molecules [46]. The kinetic energy operator is obtained numerically as a formally exact expansion in inverse powers of the stretching coordinates r_i ($i = 1, 2$), i.e. $1/r_i$ and $1/r_i^2$, about a non-rigid reference configuration [47] defined by the ρ_i grid points.

To ensure compatibility with the TROVE internal coordinate representation, the PES40K was re-expanded about the same non-rigid configuration in terms of the coordinate $1 - \exp[-(r - r_e)]$ up to eighth order. Here r_e = 0.958649 Å is the equilibrium parameter used in the PES40K definition.

TROVE employs a multilayer contraction scheme (see, e.g., Tennyson and Yurchenko [48]). In step 1, primitive stretching and bending basis functions are obtained by solving the associated one-dimensional (1D) Schrödinger equations. The two equivalent stretching problems were solved on a grid of 3000 points using the Numerov–Cooley approach [49,50]. For the bending mode, associated Laguerre polynomials L_v^l were used and optimized for the corresponding 1D Schrödinger equation on a grid of 12 000 points; here v and l denote the bending vibrational and vibrational angular momentum quantum numbers, respectively. The bending 1D Hamiltonian includes the k-dependent centrifugal-distortion term. For each 1D model Hamiltonian (stretch or bend), the remaining coordinates were fixed at their equilibrium values.

In step 2, the 1D basis functions were used to solve reduced vibrational problems for the 2D stretching and 1D bending subspaces. These reduced Hamiltonians were constructed by averaging the full 3D vibrational ($J = 0$) Hamiltonian over the appropriate ground-state basis functions. The resulting eigenfunctions were symmetrized using the automatic symmetry-adaptation procedure [51] and combined to form the contracted 3D vibrational basis for the final $J = 0$ calculation

(step 3). The 'artificial extended molecular' symmetry group C_{2n}(AEM) with $n = 30$ [52] was adopted in the TROVE calculations, and the resulting rovibrational states were subsequently mapped onto the irreducible representations of the standard C_{2v}(M) molecular symmetry group [53].

The $J = 0$ eigenfunctions were then used to construct rovibrational basis sets for $J > 0$, with the rotational part represented by symmetrized rigid-rotor functions [54]. The primitive basis sets were truncated using $v_{\max}^{\mathrm{str}} = 36$ for stretches and $v_{\max}^{\mathrm{bend}} = 52$ for the bend, with the vibrational angular momentum quantum number l in L_v^l limited by $l_{\max} = 30$. The same atomic masses as in the DVR3D calculations described above were employed. The $J = 0$ contraction was controlled by an energy cutoff of $E = 70\,000$ cm^{-1}.

Rovibrational states generated with TROVE are uniquely labeled by the rotational quantum number J, the total symmetry Γ of the molecular symmetry group, and the eigenstate counting number λ (ordered by increasing energy). Each state can be further associated with approximate quantum numbers v_1, v_2, v_3 determined from the dominant basis-function contribution [45]. Energies for all states up to $J = 60$ were generated and used for correlation with the DVR3D energies.

3. Comparison of line positions and intensities with experiment and calculations

The calculated intensities of the UCLH2O296 line list were compared with HITRAN2020 for lines below 27 000 cm^{-1}. In this range, HITRAN2020 contains 274 768 lines for $H_2{}^{16}O$ with intensities mostly stronger than 10^{-30} cm/molecule. Below 2000 cm^{-1} there are 250 lines weaker than this cutoff which are not consider here. The UCLH2O296 line list contains 271 257 lines stronger than 10^{-30} cm/molecule at the HITRAN temperature of 296 K. We note that the UCLH2O296 line list was calculated with the same DMS [43] as used to give HITRAN2020 line intensities when no better source was available. However, UCLH2O296 used wavefunctions obtained using the PES40K potential obtained in this work. There are therefore reasons to expect similar line intensities for many transitions in both line lists. Larger differences occur for lines with states involved in resonances [55] and for weak lines with intensities near the cut-off threshold. Comparison shows that the intensities of 109 253 (40%) lines agree to better than 1%, 67 029 (25%), agree to between 1 and 5%, 57 733 (20%), agree to between 5%–20%, 34 057 (12%), agree to between 20 and 50%, while the remaining 6539 (3%) of line we could match disagree by more than 50%. This gives a total of 274 611 lines, slightly more than the number, 271 257, in our line list. This difference is likely due to small differences in the intensity of lines near the intensity cutoff of 10^{-30} cm/molecule. A detailed comparison of HITRAN2020 and UCLH2O296 line lists' intensities in the range 0–27 000 cm^{-1} is given in the supplementary materials. For comparison of intensities between HITRAN and UCLH2O296 the later was scaled to natural abundance.

4. Labeling of the energy levels

Here we employ three different approaches to try to determine the most appropriate quantum numbers with which to label each energy level. An important consideration is that each label should be unique: no two energy levels should share the same label; this rule is enforced below. Traditional methods of energy levels labeling, based on smooth variation of the energy on quantum numbers, work well for small values of quantum numbers, but fail as vibrational or rotational quantum numbers increase. See, for example, Figure 1 of Polyansky et al. [56] for an example of the second (1ν) polyad, or our Fig. 2 for an example of the fifth ($2\nu + \delta$) polyad. Therefore, labeling methods based on wave function analysis are more reliable, and the smooth dependence of energy levels on quantum numbers should be used only for minor corrections in the analysis of wave functions.

Table 2
TROVE and MARVEL match and unmatch statistics; upper half: levels below 10 000 cm^{-1}; lower half: levels in the 10 000–25 000 cm^{-1} energy range.

J =	0–5	6–10	11–15	16–20
K_a match	763	1402	1068	424
K_a unmatch	3	87	399	555
K_c match	765	1403	1071	424
K_c unmatch	1	86	396	555
v_1 match	763	1471	1432	961
v_1 unmatch	3	18	35	18
v_2 match	766	1473	1433	957
v_2 unmatch	0	16	34	22
v_3 match	763	1486	1462	978
v_3 unmatch	3	3	5	1
K_a match	2570	3327	1478	741
K_a unmatch	94	561	765	887
K_c match	2619	3474	1506	768
K_c unmatch	45	414	737	860
v_1 match	2340	3111	2039	1539
v_1 unmatch	324	777	204	89
v_2 match	2372	3245	2089	1562
v_2 unmatch	292	643	154	66
v_3 match	2524	3511	2118	1551
v_3 unmatch	140	377	125	77

4.1. Wavefunction contribution

Our vibrational labeling for $H_2{}^{16}O$ started from TROVE assignment, which uses the largest contribution concept, where the eigen states are assigned vibrational quantum numbers that correspond to the largest basis set contribution. The method is described in detail on p 121, Section 5.4.4 of Yurchenko [57]. Only levels with $J = 0, \ldots, 20$ were passed through this procedure, and the number of labels (each quantum number separately) that matched and did not match the labeling provided by the MARVEL procedure is given in Table 2. Levels which are not determined using the MARVEL results are not presented in Table 2. From Table 2 it is evident that the accuracy of vibrational labeling is higher than that of rotational ones, and the accuracy of both of these decreases with increasing energy.

4.2. Nodes counting

Vibrational quantum numbers should reflect a wave function structure of an excited state. In the harmonic oscillator approximation, using a $J = 0$ wavefunctions, a number of wave function nodes in each coordinate direction are strictly equal to corresponding quantum numbers, while for a real molecule such equality becomes approximate. However, as shown in Table 3, vibration levels with energies below 10 000 cm^{-1} could be assigned this way. At higher energies, the bending labeling accuracy for v_2 remains good, while stretching labeling becomes unreliable. One of the possible explanations of that is that for higher energies the behavior of the modes changes from the normal to local character. For this reason we only used v_2 node labeling when manually correcting the vibrational labels. The structure of the rovibrational wavefunction significantly differs from the vibrational one because of complicated mixing, that is why we use the node labeling method only for $J = 0$ states.

4.3. Modified Hose-Taylor method

The original application of the Hose-Taylor theorem [30] to $H_2{}^{16}O$ by Conway et al. [28] was based on computation of the integral

$$I(J,k) = \int |\langle \Psi(J,k,\xi)^2 \rangle| d\xi, \tag{2}$$

for each value of the k quantum number used by DVR3D to characterize rotational basis functions along the axis perpendicular to the bisector of the $\widehat{\mathrm{HOH}}$ angle and ξ is the set of all internal coordinates. The

Table 3
Nodes labeling and MARVEL match and unmatch vibrational statistics; column 2: levels below 10 000 cm^{-1}; column 3: levels in the 10 000–25 000 cm^{-1} energy range.

Label	E low	E high
υ_1 match	23	31
υ_1 unmatch	0	31
υ_2 match	23	58
υ_2 unmatch	0	4
υ_3 match	23	48
υ_3 unmatch	0	14

hose_taylor program of Conway et al. [28] finds the largest component $I(J,k)$, and then labels the level under consideration with this k, assuming $k = K_a$; K_c can then be uniquely defined using J, K_a and symmetry. The assumption that $K_a \simeq k$ is endorsed by the work of Szidarovszky et al. [34].

Our modified method provides not only rotational labeling but also bending labeling. To do that, the wavefunction is represented as a function of rotational quantum number J, rotational projection k, bending angle θ (defined in Radau coordinates) and stretching vibrational coordinates ξ_s. We then calculated the θ-dispersion for each wavefunction as given by

$$D(J,k) = \int (\theta - \theta(J,k)_{exp})^2 \Psi(J,k,\theta,\xi_s)^2 d\theta d\xi_s, \quad (3)$$

where $\theta(J,k)_{exp}$ provides a J- and k-dependent expectation value of θ:

$$\theta(J,k)_{exp} = \int (\theta |\Psi(J,k,\theta,\xi_s))^2 | d\theta d\xi_s. \quad (4)$$

The original Hose–Taylor integrals $I(J,k)$ are used to split the set of DVR3D states with fixed J and symmetry into rotational subsets with fixed k index for every subset. So, every state is supplemented by a k_{HT} intermediate label. If a state under consideration is a first state (a lowest state), which falls into a certain rotational J and k_{HT} subset, then the bending $D(J,k_{HT})$ integral of that state is stored as a normalization coefficient for a given J and k_{HT} subset considered. If a subsequent state also falls into a subset (J, k_{HT}) with the $D(J,k_{HT})$ integral value being larger than all previous integral values in the same J, k_{HT} subset, then it is used to correct the specific subset normalization. Normalization and correction coefficients together form piecewise linear scales, used to convert all $D(J,k)$ integrals to usually near-integer quasi-quantum numbers, which are summed up by the k index and then rounded to estimate the bending quantum number, υ_2.

A second modification of the Hose_Taylor program of Conway et al. [28] focuses on rotational labeling. The original method assumes that rotational basis functions are eigenfunctions of K_a and K_c quantum numbers (as in the TROVE labeling method). Our detailed analysis of pure rotational state's wavefunctions showed that the decomposition coefficients differ significantly both from unity and zero. Our modified labeling method builds a set of sample value of rotational decomposition coefficients of pure rotational states, which are then compared to the rotational decomposition coefficients of all other states to differentiate the pure rotational states from vibrationally excited states with the rotational part highly correlated to one of the sample pure rotational states. Table 4 shows the labeling statistics of using our modified Hose-Taylor method. For this method, the accuracy of the rotational labeling is better than that of the vibrational labeling. This is opposite to the TROVE labeling scheme, which degrades with increasing energy both for rotational and vibrational quantum numbers.

4.4. Labeling merging and correction

Analysis of Tables 2 and 4 shows that vibrational labeling using the TROVE method is more accurate, while rotational labeling is more accurate using the modified Hose-Taylor method. Therefore our first synthetic labeling takes the vibrational labels from TROVE, while rotational labels are from the modified Hose-Taylor calculations. These predicted labels are then overwritten by the MARVEL labels, if available.

Table 4
Match/unmatch comparison between the results of our modified Hose-Taylor procedure and MARVEL labels; upper half: levels below 10 000 cm^{-1}; lower half: levels in the 10 000–25 000 cm^{-1} energy range.

J =	0–5	6–10	11–15	16–20	21–25	26, 27
K_a match	765	1462	1402	944	414	59
K_a unmatch	1	27	65	35	3	0
K_c match	765	1465	1406	946	414	59
K_c unmatch	1	24	61	33	3	0
υ_2 match	734	1398	1306	933	415	59
υ_2 unmatch	32	91	161	46	2	0
K_a match	2592	3465	1922	1371	1240	328
K_a unmatch	72	423	321	257	347	222
K_c match	2640	3613	1966	1391	1259	333
K_c unmatch	24	275	277	237	328	217
υ_2 match	128	341	304	569	864	348
υ_2 unmatch	1482	3547	1939	1059	723	202

Next step is to consider states with duplicate labels. The levels concerned were first examined using the υ_2 label provided by our modified Hose-Taylor computation. Only one state with the duplicated labels was retained, while for the other states the υ_2 label was taken from the modified Hose-Taylor calculation, and υ_1 and υ_3 were marked as unknown. Unknown vibrational quantum numbers are denoted as −2, while rotational are denoted as −1, −2, −3 and −4 for A_1, A_2, B_1 and B_2 irreducible representations respectively.

4.5. Correction by $E(K_a)$ dependencies

Typical molecular line lists provide ro-vibrational energies and associated quantum numbers that allow determination of transition wavenumbers and the unique assignment of the upper and lower states by vibrational and rotational quantum numbers (VRQNs) for any associated transitions. Here the energies are taken from the W2024 MARVEL data for $H_2{}^{16}O$ [1] augmented with the ab initio data of this work. Errors in the assignment of the upper/lower states lead to errors in the VRQNs labeling of associated transitions. The labeling of states can be checked using the smooth variation and pairing rules of Ma et al. [58]. For a given vibrational state, plots were made for each J of the term value versus K_a. If the assignment of each term value is correct, the curves corresponding to symmetric and antisymmetric states demonstrate pairing and vary smoothly. The upper panel of Fig. 1 shows the term values for different rotational states with $J = 13$ of the (040) vibrational state. The plot shows that the 13_{85} and 13_{86} states are not correctly assigned. These states, being some 4000 cm^{-1} too high belong to a different vibrational state. Two iterations of this procedure were carried out, which led to the labeling of energy levels and spectrum published in this work. The lower panel of Fig. 1 shows the final term values of the $J = 13$ (040) states. The corrected data vary smoothly and follow the pairing rule. However, this procedure requires a lot of manual work due to the high density of energy levels and thus the associated assignemment is be to be continued in subsequent work. A list of calculated energy levels (with the corresponding MARVEL assignment and energies) is provided in the supplementary materials.

4.6. Fifth polyad ($2\nu + \delta$)

The fifth polyad of $H_2{}^{16}O$ contains six vibrational states (050), (130), (031), (210), (111) and (012) and is conventionally denoted $2\nu + \delta$; these states interact with each other causing accidental resonances between certain rotation states with the same overall symmetry.

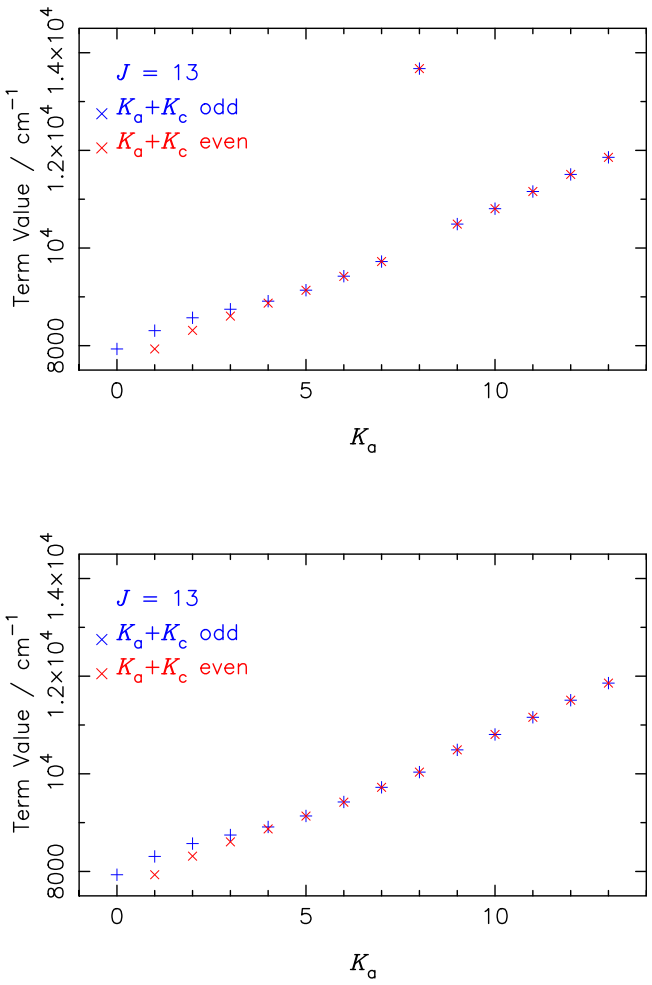

Fig. 1. Term values for the $J = 13$ states of the (040) vibrational state versus K_a; upper panel: initial set; lower panel: after two iterations of correcting using the smooth variation and pairing rules. Shown are the even states (red vertical crosses) and the odd states (blue diagonal crosses). The 13_{85} and 13_{86} states are not correctly assigned in the initial set (upper panel) but corrected in the final set (lower panel).

Fig. 2 illustrates the relative position of the $K_a = J$ levels for these six vibrational states; sharp structures due to the levels interacting with each other for K_a between 8 and 11 can be clearly seen. The mixing of wave functions leads to a visible shift in energies on the graph; however, in the example considered, it hardly interferes with the labeling. All levels shown in the figure for $J \leq 8$ are presented in the MARVEL dataset, but for $J \geq 13$, only the state (111) is present. For $J = 9$ to 12, the levels shown are only partially provided by the MARVEL dataset, however, the analysis conducted in this work has allowed us to successfully fill the gaps even in a region of strong interaction.

5. Line shape data

The air-broadened half-width, γ_{air}, the air-induced pressure shift, δ_{air}, the temperature dependence of the air-broadened half-width, n_{air}, and the self-broadened half-width, γ_{self} were added to the UCLH2O296 line file using the HITRAN "diet" procedure [59]. The procedure contains three tiers of measurement data files for addition to the water vapor transitions. First, data of known high precision for γ_{air} and δ_{air} were extracted from an updated version of the measurement database of Gamache and Hartmann [60] and put into a "priority data" file.

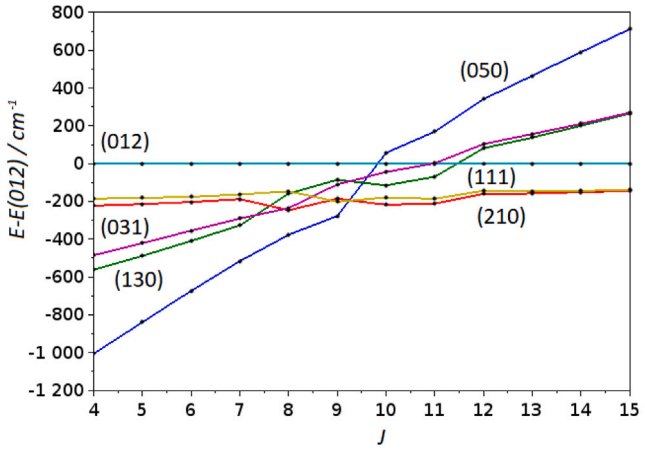

Fig. 2. Energy levels with $J = K_a$ as a function of J for the (050), (130), (031), (210), (111), and (012) vibrational states (5th polyad). For each value of J, the zero of energy is taken as the J_{J0} of the (012) state.

Next, an intercomparison of the air-broadening measurement data was done after filtering out references with inconsistent data. The average values from the intercomparison of data were determined and stored in files for the half-widths and the line shifts. A similar procedure was done for the self-broadened data. In the 3rd tier, lines in the measurement database that contain only a single datum for a transition were written to separate files for the half-widths and the line shifts.

The next tier in the "diet" procedure is the use of Complex Robert Bonamy-Ma (CRBM) calculations of the line shape parameters. Taking the CRBM calculations of Vispoel et al. [61] for the H_2O–N_2 collision system and CRBM calculations of Gamache et al. [62] for the H_2O–O_2 collision system, the line shape information for the H_2O-air collision system were computed using $\gamma_{\text{air}} = 0.79\gamma_{N_2} + 0.21\gamma_{O_2}$ with a similar formula for the line shift. The CRBM calculations considered 13 temperatures from 200–3000 K; γ_{air} and δ_{air} were determined for all temperatures so that the temperature dependence could be determined. The CRBM calculations were made for 10 782 rotational transitions for the rotational band and for bands with 1–4 υ_1, υ_2, and υ_3 vibrational quanta exchanged, giving some 140 thousand calculated transitions. These data make up the calculated H_2O-air line shape files for the $H_2{}^{16}O$. The theoretical calculations make up the 4th tier of the "diet" procedure. The 5th tier of the "diet" procedure is the use of predicted values of γ_{air}, δ_{air}, and the temperature dependence of each determined using equations derived by Gamache and Hartmann [63] that can accurately predict γ_{air} and δ_{air} [63] at any temperature. The prediction routine has been successfully applied to H_2O-air by Jacquemart et al. [64], to CO_2-x, where x = N_2, O_2, air, CO_2 by Gamache and Lamouroux [65], to H_2O–H_2 by Gamache et al. [66], and to H_2O–N_2 by Vispoel et al. [67] and the predicted values agree well with the calculated or measured ones with a standard deviation 5% for the H_2O studies and 1% for the CO_2 studies. Here, using the CRBM data, a prediction routine was developed based on the $H_2{}^{16}O$-air CRBM data and the prediction coefficients determined at the 13 temperatures allowing the temperature dependence to also be determined. These data make the predicted part of the H_2O-air database. For transitions that are not in the above databases, the half-width is estimated by using the rotation band value if it is available, i.e. neglecting vibrational dependence. However, there still remain a large number of H_2O transition that do not have attributions. These are transitions generated from ab initio calculations were only the rotational quantum number J and parity are true quantum numbers. For these transitions, the rotation band calculations were taken and half-widths as a function of J'' were determined. These data were extrapolated to $J'' = 50$. Note, because of the very strong vibrational dependence of the line shift, no comparable

Table 5
Summary of added line shape information to the UCLH2O296 H_2O line file.

"diet" tier	γ_{air}	δ_{air}	n_{air}	γ_{self}
Priority data	4 680	3 599	4 358	0
Intercomparison data	2 629	701	249	5 359
Singles data	5 419	3 275	33	16 923
CRBM data	40 534	42 224	42 861	1 611
Predicted data	171 119	174 505	176 572	0
J averaged data	253 014	0	253 322	453 502

average values can be determined. These data are the last (6th) tier of the "diet" procedure for line shape information. The "diet" data sets were taken and for each tier python dictionaries were made using the VRQNs as the key. These data are then added to the ExoMol H_2O line file using a python algorithm that reads the water vapor line file and using the VRQNs and selectively adds the line shape data from the dictionaries to each transition in the prioritized scheme discussed above. The summary of adding the line shape data is presented in Table 5. Data were added to 477 395 water vapor transitions.

It is well known that the power-law temperature dependence of the half-width does not work for all ro-vibrational transitions of water vapor [68]. Using the two-term approximation of the Gamache–Vispoel law [68] (often called the Double Power Law, DPL), the temperature dependence of the half-width and line shift are

$$\gamma(T) = c_1 \left[\frac{T_r}{T}\right]^{n_1} + c_2 \left[\frac{T_r}{T}\right]^{n_2} \quad (5)$$

and

$$\delta(T) = d_1 \left[\frac{T_r}{T}\right]^{n_{\delta 1}} + d_2 \left[\frac{T_r}{T}\right]^{n_{\delta 2}}. \quad (6)$$

In these equations, γ, δ, c_1, c_2, d_1 and d_2 are in cm^{-1} atm^{-1}, T is in K and T_r is the reference temperature, here 296 K. The DPL coefficients were determined for the transitions considered in the CRBM calculations and for the predicted transitions. The coefficients are valid from 200–3000 K. In total, DPL coefficients were added to 46 340 transitions from the CRBM data and to 178 043 transitions from the predicted data. The calculated line shape parameters can be found in the UCLH2O296 line list.

6. Conclusions

The key importance of the spectrum of the water molecule requires ongoing improvements in the accuracy and completeness of water spectral line lists. We presented here an $H_2{}^{16}O$ line list computed using an improved accuracy PES: keeping the same accuracy as our best PES15K potential in the region up to 15 000 cm^{-1}, twofold more accurate than the POKAZATEL PES for medium energies from 15 000 and up to 25 000 cm^{-1}, and almost as accurate for high energies, and the most accurate *ab initio* DMS [43] currently available. We have significantly extended the rotation-vibration labeling of the energy levels: 92 035 levels are now labeled by K_a, K_c and v_2 quantum numbers, and 48 440 of these 92 035 levels were labeled fully by K_a, K_c, v_1, v_2 and v_3. The line positions and line intensities with the rotational and vibrational quantum numbers of the energy levels involved in the line centers are compared with the known experimental and experimentally derived data, taken from the W2024 MARVEL study [1] and the HITRAN database. Line positions are improved by the more accurate PES and more extensive use of MARVEL energy levels (MARVELisation). The more accurate PES results in better wavefunctions and hence improved intensities. An important part of the line list are the lineshape parameters, especially the linewidth. An extension of this information in comparison with the data published in the literature is presented. Thus extending range of the line list. The greatly extended uses of reliable rotational and vibrational labels, extended line shape data, more accurate line positions and intensities means that the UCLH2O296 line list should represent a significant improvement over the existing line lists.

CRediT authorship contribution statement

Nikolai F. Zobov: Writing – original draft, Supervision, Methodology, Investigation, Funding acquisition, Formal analysis, Data curation. **Irina I. Mizus:** Writing – review & editing, Validation, Investigation, Data curation. **Roman I. Ovsyannikov:** Writing – review & editing, Methodology, Investigation, Formal analysis, Data curation. **Mikhail A. Rogov:** Writing – review & editing, Investigation, Data curation. **Jonathan Tennyson:** Writing – review & editing, Software, Funding acquisition. **Marco Pezzella:** Methodology, Data curation. **Sergei N. Yurchenko:** Software, Investigation, Formal analysis. **Robert R. Gamache:** Writing – review & editing, Methodology, Investigation, Formal analysis, Data curation. **Oleg L. Polyansky:** Writing – original draft, Supervision, Methodology, Funding acquisition, Formal analysis.

Declaration of competing interest

The authors declare no conflict of interest.

Acknowledgment

This work was supported by the Ministry of Science and Higher Education of the Russian Federation. We acknowledge support by State Project IAP RAS No. FFUF-2024-0016, ERC Advanced Investigator grants 883830, and STFC, United Kingdom grants UKRI/ST/B001183/1 and ST/Y001508/1 for supporting aspects of this project. O.L.P. acknowledges support from QuantumPascalproject 18SIB04, which has received funding from the EMPIR, Germany programme co-financed by the Participating States and from the European Union's Horizon 2020 research and innovation programme.

Appendix A. Supplementary data

Supplementary material related to this article can be found online at https://doi.org/10.1016/j.jqsrt.2026.109833.The data associated with this article are provided in the supplementary materials.

Data availability

The data associated with this article are provided in the paper and the supplementary materials. In addition, The UCLH2O296 line list is available in both ExoMol [69] and HITRAN [70] formats on the ExoMol website (www.exomol.com).

Supplementary material related to this article can be found online at https://doi.org/10.1016/j.jqsrt.2025.109620.

References

[1] Furtenbacher T, Tóbiás R, Tennyson J, Gamache RR, Császár AG. Sci Data 2024;11:1058.
[2] Furtenbacher T, Császár AG, Tennyson J. J Mol Spectrosc 2007;245:115.
[3] Tennyson J, Furtenbacher T, Yurchenko SN, Császár AG. J Quant Spectrosc Radiat Transfer 2024;316:108902.
[4] Tennyson J, Bernath PF, Brown LR, Campargue A, Carleer MR, Császár AG, Daumont L, Gamache RR, Hodges JT, Naumenko OV, et al. J Quant Spectrosc Radiat Transfer 2013;117:29.
[5] Tennyson J, Bernath PF, Brown LR, Campargue A, Császár AG, Daumont L, Gamache RR, Hodges JT, Naumenko OV, Polyansky OL, et al. Pure Appl Chem 2014;86:71.
[6] Tóbiás R, Furtenbacher T, Tennyson J, Császár AG. Phys Chem Chem Phys 2019;21:3473.
[7] Furtenbacher T, Tóbiás R, Tennyson J, Polyansky OL, Császár AG. J Phys Chem Ref Data 2020;49:033101.
[8] Furtenbacher T, Tóbiás R, Tennyson J, Polyansky OL, Kyuberis AA, Ovsyannikov RI, Zobov NF, Császár AG. J Phys Chem Ref Data 2020;49:043103.
[9] Tennyson J, Bernath PF, Brown LR, Campargue A, Carleer MR, Császár AG, Gamache RR, Hodges JT, Jenouvrier A, Naumenko OV, et al. J Quant Spectrosc Radiat Transfer 2009;110:573.

[10] Abdoulanziz A, Argentin C, Laporta V, Chakrabarti K, Bultel A, Tennyson J, Schneider IF, Mezei JZ. J Appl Phys 2021;129:053303.
[11] Polyansky OL, Jensen P, Tennyson J. J Mol Spectrosc 1996;178:184.
[12] Partridge H, Schwenke DW. J Chem Phys 1997;106:4618.
[13] Shirin SV, Polyansky OL, Zobov NF, Ovsyannikov RI, Császár AG, Tennyson J. J Mol Spectrosc 2006;236:216.
[14] Bubukina II, Zobov NF, Polyansky OL, Shirin SV, Yurchenko SN. Opt Spectrosc 2011;110:160.
[15] Mizus II, Kyuberis AA, Zobov NF, Makhnev VY, Polyansky OL, Tennyson J. Phil Trans R Soc Lond A 2018;376:20170149.
[16] Tóbiás R, Furtenbacher T, Császár AG, Naumenko OV, Tennyson J, Flaud J-M, Kumard P, Poirier B. J Quant Spectrosc Radiat Transfer 2018;208:152.
[17] Barber RJ, Tennyson J, Harris GJ, Tolchenov RN. Mon Not R Astron Soc 2006;368:1087.
[18] Polyansky OL, Kyuberis AA, Zobov NF, Tennyson J, Yurchenko SN, Lodi L. Mon Not R Astron Soc 2018;480:2597.
[19] Tinetti G, Vidal-Madjar A, Liang M-C, Beaulieu J-P, Yung Y, Carey S, Barber RJ, Tennyson J, Ribas I, Allard N, et al. Nature 2007;448:169.
[20] Schwenke DW, Partridge H. J Chem Phys 2000;113:6592.
[21] Conway EK, Gordon IE, Kyuberis AA, Polyansky OL, Tennyson J, Zobov NF. J Quant Spectrosc Radiat Transfer 2020;241:106711.
[22] Conway EK, Gordon IE, Tennyson J, Polyansky OL, Yurchenko SN, Chance K. Atmos Chem Phys 2020;20:10015.
[23] Rothman LS, Gordon IE, Babikov Y, Barbe A, Benner DC, Bernath PF, Birk M, Bizzocchi L, Boudon V, Brown LR, et al. J Quant Spectrosc Radiat Transfer 2013;130:4.
[24] Gordon IE, Rothman LS, Hill C, Kochanov RV, Tan Y, Bernath PF, Birk M, Boudon V, Campargue A, Chance KV, et al. J Quant Spectrosc Radiat Transfer 2017;203:3.
[25] Gordon IE, Rothman LS, Hargreaves RJ, Hashemi R, Karlovets EV, Skinner FM, Conway EK, Hill C, Kochanov RV, Tan Y, et al. J Quant Spectrosc Radiat Transfer 2022;277:107949.
[26] Viti S, Tennyson J, Polyansky OL. Mon Not R Astron Soc 1997;287:79.
[27] Mátyus E, Fabri C, Szidarovszky T, Czako G, Allen WD, Császár AG. J Chem Phys 2010;133:034113.
[28] Conway EK, Gordon IE, Hargreaves RJ, Gamache RR, Polyansky OL, Tennyson J. J Quant Spectrosc Radiat Transfer 2021;270:107716.
[29] Yurchenko S, Thiel W, Jensen P. J Mol Spectrosc 2007;245:126.
[30] Hose G, Taylor HS. Phys Rev Lett 1983;51:947–50.
[31] Carleer M, Jenouvrier A, Vandaele A-C, Bernath PF, Mérienne MF, Colin R, Zobov NF, Polyansky OL, Tennyson J, Savin VA. J Chem Phys 1999;111:2444.
[32] Tolchenov RN, Naumenko O, Zobov NF, Shirin SV, Polyansky OL, Tennyson J, Carleer M, Coheur P-F, Fally S, Jenouvrier A, et al. J Mol Spectrosc 2005;233:68.
[33] Császár AG, Mátyus E, Szidarovszky T, Lodi L, Zobov NF, Shirin SV, Polyansky OL, Tennyson J. J Quant Spectrosc Radiat Transfer 2010;111:1043.
[34] Szidarovszky T, Fábri C, Császár AG. J Chem Phys 2012;136:174112.
[35] Zobov NF, Ovsyannikov RI, Shirin SV, Polyansky OL. Opt Spectrosc 2007;102:348.
[36] Smydke J, Csaszar AG. Mol Phys 2019;117:1682.
[37] Child MS, Halonen L. Adv Chem Phys 1984;57:1.
[38] Zobov NF, Shirin SV, Polyansky OL, Tennyson J, Coheur P-F, Bernath PF, Carleer M, Colin R. Chem Phys Lett 2005;414:193.
[39] Child MS, Weston T, Tennyson J. Mol Phys 1999;96:371.
[40] Varandas AJC. J Chem Phys 1996;105:3524.
[41] Tennyson J, Kostin MA, Barletta P, Harris GJ, Polyansky OL, Ramanlal J, Zobov NF. Comput Phys Comm 2004;163:85.
[42] Yurchenko SN, Carvajal M, Jensen P, Herregodts F, Huet TR. JCP 2003;290:59.
[43] Conway EK, Kyuberis AA, Polyansky OL, Tennyson J, Zobov N. J Chem Phys 2018;149:084307.
[44] McKemmish LK, Bowesman CA, Kefala K, Perri AN, Syme AM, Yurchenko SN, Tennyson J. RAS Tech Instr 2024;3:565.
[45] Yurchenko SN, Thiel W, Jensen P. J Mol Spectrosc 2007;245:126.
[46] Yurchenko SN, Mellor TM. J Chem Phys 2020;153:154106, URL https://doi.org/10.1063/5.0019546.
[47] Hougen JT, Bunker PR, Johns JWC. J Mol Spectrosc 1970;34:136.
[48] Tennyson J, Yurchenko SN. Int J Quantum Chem 2017;117:92.
[49] Noumerov BV. Mon Not R Astron Soc 1924;84:592.
[50] Cooley JW. Math Comp 1961;15:363.
[51] Yurchenko SN, Yachmenev A, Ovsyannikov RI. J Chem Theory Comput 2017;13:4368.
[52] Mellor TM, Yurchenko SN, Jensen P. Symmetry 2021;13:548.
[53] Bunker PR, Jensen P. Molecular symmetry and spectroscopy. 2nd ed.. Ottawa, Canada: NRC Research Press; 2006.
[54] Yurchenko SN, Yachmenev A, Ovsyannikov RI. J Chem Theory Comput 2017;13:4368, http://dx.doi.org/10.1021/acs.jctc.7b00506.
[55] Lodi L, Tennyson J. J Quant Spectrosc Radiat Transfer 2012;113:850.
[56] Polyansky OL, Tennyson J, Bernath PF. J Mol Spectrosc 1997;186:213.
[57] Yurchenko S. Computational spectroscopy of polyatomic molecules. CRC Press; 2023.
[58] Ma Q, Tipping R, Lavrentieva N. Mol Phys 2011;109:1925.
[59] Gordon I, Rothman L, Gamache R, Jacquemart D, Boone C, Bernath P, Shephard M, Delamere J, Clough S. J Quant Spectrosc Radiat Transfer 2007;108:389.
[60] Gamache R, Hartmann J-M. Can J Chem 2004;82:1013.
[61] Vispoel B, Cavalcanti J, Gamache R. J Quant Spectros Radiat Transf 2019;228:79.
[62] Gamache RR, Orphanos N, Vispoel B, Sung K, Toon G. Mol Phys 2023;e2281592:1.
[63] Gamache R, Hartmann J-M. J Quant Spectrosc Radiat Transfer 2004;83:119.
[64] Jacquemart D, Gamache R, Rothman L. J Quant Spectrosc Radiat Transfer 2005;96:205.
[65] Gamache R, Lamouroux J. J Quant Spectrosc Radiat Transfer 2013;130:158.
[66] Gamache R, Vispoel B, Renaud C, Cleghorn K, Hartmann L. Icarus 2019;326:186.
[67] Vispoel B, Cavalcanti J, Paige E, Gamache R. J Quant Spectros Radiat Transf 2019;252:107030.
[68] Gamache R, Vispoel B. J Quant Spectros Radiat Transf 2018;217:440.
[69] Tennyson J, Hill C, Yurchenko SN. 6th international conference on atomic and molecular data and their applications ICAMDATA-2012. AIP conference proceedings, vol. 1545, AIP, New York; 2013, p. 186–95.
[70] Rothman LS, Jacquemart D, Barbe A, Benner DC, Birk M, Brown LR, Carleer MR, Chackerian C, Chance K, Coudert LH, et al. J Quant Spectrosc Radiat Transfer 2005;96:139.